2D and 3D gust response using a prescribed velocity method in viscous flows

S. J. Huntley*, D. Jones† and A. Gaitonde†

Department of Aerospace Engineering, University of Bristol, Bristol, BS8 1TR, United Kingdom

Results are presented for the interaction between a wide body aircraft and a gust using the split velocity method, which has been extended to viscous flows. The method is first demonstrated for two dimensions on a NACA 0012 aerofoil before being extended to the 3D case. In both instances a series of 1-Cosine gusts were used to compare solutions between the split velocity method and, another prescribed velocity method, the field velocity method. The field velocity method is shown to be a simplification of the split velocity method, with the latter requiring extra source terms that account for the interaction of the aerofoil on the gust. It was found that the differences were small for longer wavelength gusts but at shorter wavelengths the gradients become larger and the split velocity method produces more accurate results.

Nomenclature

$\hat{u}, \hat{v}, \hat{w}$	gust velocity components
γ	ratio of specific heats
μ	dynamic viscosity
ρ	density
$\tilde{u}, \tilde{v}, \tilde{w}$	background velocity components
c	chord length
E	energy
p	pressure
Pr	Prandtl number
Re	Reynolds number
s	non-dimensional time
t	time
u, v, w	total velocity components
u_{ref}	freestream velocity
x_t, y_t, z_t	grid velocities

I. Introduction

Unsteady load calculations play a crucial role in aircraft design and determine critical load cases that affect structural design, control systems and performance. These loads are defined by Certification Authorities (FAR/JAR 25 for large commercial aeroplanes) and require aircraft to withstand them for various flight conditions. Gusts are often the most critical load case for structural design and fatigue calculations,[1] and are determined by dynamic analysis to include unsteady aerodynamic effects. Aerofoil behaviour in gusts has been studied in the past using accelerometers fitted to aircraft and was the focus of the first ever NACA report.[2]

Loads due to gusts are therefore applied to detailed structural design during the design phase. Since the flight conditions that produce critical load cases are not known, the aerodynamic forces are calculated

*Research Assistant

†Senior Aerodynamics Lecturer

for nearly 100,000 load cases for a conventional aircraft.[1] This significantly adds to the cost of design as the analyses need to be performed for every design-iteration. At present, simplified low to medium fidelity models are used for gust modelling. In early design stages, the unsteady 2D strip theory approach is used with indicial lift functions (e.g. Wagner, Kssner functions[3]) for gust responses in the time-domain. While this method is computationally inexpensive, it is of low fidelity and neglects three-dimensional effects such as tip effects and wake-lifting surface interactions.

For low subsonic speeds, aerodynamic forces can be accurately predicted using the three-dimensional unsteady doublet lattice method (DLM)[4,5] which is widely used in industry. DLM is a three-dimensional unsteady potential-flow method that incorporates tip effects and wake interference. In the steady case, where reduced frequency is zero, DLM reduces to the steady Vortex Lattice Method (VLM).[5] Unlike the VLM which solves the velocity potential equations, DLM solves acceleration potential equations using a harmonic approach leading to solutions in the frequency-domain.[4] When performing gust calculation in the time-domain, the aerodynamic influence coefficient (AIC) resulting from DLM must be converted into the time-domain from the frequency-domain using the rational fraction approximation (RFA).[6] However, since DLM is a linear method, it does not accurately predict transonic regions where aerodynamic non-linearities are present and compressibility corrections, like the Prandtl-Glauert correction, are limited. Steady CFD solutions and wind tunnel data are obtained for accurate prediction in transonic regions and are used to correct the panel method solutions. These form the current industry best practice for gust calculations.[7]

High fidelity CFD solutions are sought during the detailed design stages for accurate results for cruise, as well as to correct panel method solutions for non-linearities. Despite the already high computational cost associated with CFD simulations, the accuracy achievable for unsteady applications is limited by numerical dissipation and stability constraints.[8] The numerical dissipation associated with CFD is particularly poor at regions with insufficient grid resolution, such as far field upstream, where disturbances, such as gusts or vortices, diffuse rapidly.[9] Increasing the grid resolution by employing a fine mesh throughout the computation domain allows for some accuracy in the solution, but adds to the computational cost rendering them impractical for design. One possible solution to this problem is to locally refine or redistribute grid points as the disturbances convect through the domain to preserve its spatial resolution.[10] However, this requires a grid generator to refine the meshes locally or in the two-step redistribution method, an elliptical approach for grid adaptation where a high-order polynomial interpolation to redistribute baseline mesh is needed for accurate results.[11] This adds to the computational cost, and affects the grid quality from distortion thus requiring relatively fine initial mesh. Furthermore, using this approach in a gust field would require adaptation or refinement across the normal direction, as the gust is defined by convecting disturbances from unsteady farfield boundary conditions (FBC).[12] The adaptive grid method changes the volume of grid cells as disturbances move where geometric conservation law (GCL) must be satisfied to avoid spurious source terms.[13] Alternatively a high order scheme may be employed but this limits the use of existing solvers that employ second-order accurate operators and some high-order numerical methods actually have lower spectral resolution capability.[14]

The requirement for a fine mesh in the farfield can be overcome by prescribing gust velocities and modifying grid time metrics to simulate grid motion without actually distorting the mesh.[15,16] One such method is the Field Velocity Method (FVM)[17] which could be considered as an extension of the surface transpiration method, where velocity corrections are applied throughout the flow domain rather than just on the surface.[18] This method is said to effectively decouple angle of attack response from pitch rate influence as the aerofoil is not made to pitch.[19] In FVM, the gust velocity is prescribed and the remaining flow field is solved; this eliminates numerical dissipation of the disturbances. This allows for coarser meshes to be used away from the aerofoil thus significantly reducing computational cost. This method is also cost efficient since it is based on existing Euler equations on a moving mesh codes which are easily modified with grid velocities set to minus the gust velocities. FVM has been utilized to solve sharp edged gusts,[16]model step change in flow incidence[15] and vortex interaction problems[20] and is validated by analytical solutions from piston and linear compressible theories.[15] However, while FVM accounts for the influence of the gust on the aerofoil, it does not include all interactions between them,[12] thus reducing accuracy and applicability of this method for downstream problems such as a horizontal stabilizer. The literature for this method does not describe the simplifying assumptions made nor does it consider the momentum and energy components due to the external velocity field.[18] The Split Velocity Method (SVM) is another method which prescribes gust velocities but retains all momentum and energy components by rearranging the unsteady governing equations on a fixed mesh. This results in source terms that account for all the gust-aerofoil interactions and

provides more accurate solutions. This method has been successfully implemented for inviscid flow[9] and has been shown to provide more accurate solutions for short gusts due to the effect of spatial gradients in the source terms. This present study aims to extend the Split Velocity Method to viscous flows and explore the relationship between the resulting solutions and that of FVM. The prescribed velocity methods are simulated and compared for various 1-Cosine gusts and the effect of source terms in the downstream are explored.

II. Methodology

The FVM and SVM are both prescribed velocity methods. Both use a moving mesh solver, however, the SVM requires additional source terms. It is possible to formulate the SVM in such a way that it can be shown that the FVM is a simplification of the SVM and that the source terms arising from rearranging the governing equations are neglected. Therefore, the FVM is first presented in Section II.A and then the SVM is described in Section II.B. Details of the implementation of the two methods in the CFD code TAU are given in Section II.C.

II.A. Field Velocity Method

The Field Velocity Method prescribes gust velocities by using a moving mesh Euler solver and modifying the grid time metrics so that the grid velocities are set to minus the gust velocities. In this way the grid is not actually moved and then the velocities that are computed are relative to the gust. In other words, FVM treats the problem as if the aerofoil was moving at the speed of the gust but in the opposite direction. As disturbances are prescribed, they are preserved from numerical dissipation arising from mesh coarseness. This overcomes the fine mesh requirement imposed by the Farfield Boundary Condition (FBC) method, where fine mesh is required in the entire flow field to convect disturbances without dissipating them. The FVM or the moving mesh formulation for the Navier-Stokes equations in three dimensions are given by Eq. (1).

$$\frac{\partial}{\partial t}\begin{bmatrix}\rho\\ \rho\tilde{u}\\ \rho\tilde{v}\\ \rho\tilde{w}\\ \rho E\end{bmatrix}+\frac{\partial}{\partial x}\begin{bmatrix}\rho(\tilde{u}-x_t)\\ \rho\tilde{u}(\tilde{u}-x_t)+p\\ \rho\tilde{v}(\tilde{u}-x_t)\\ \rho\tilde{w}(\tilde{u}-x_t)\\ \rho E(\tilde{u}-x_t)+p\tilde{u}\end{bmatrix}+\frac{\partial}{\partial y}\begin{bmatrix}\rho(\tilde{v}-y_t)\\ \rho\tilde{u}(\tilde{v}-y_t)\\ \rho\tilde{v}(\tilde{v}-y_t)+p\\ \rho\tilde{w}(\tilde{v}-y_t)\\ \rho E(\tilde{v}-y_t)+p\tilde{v}\end{bmatrix}+\frac{\partial}{\partial z}\begin{bmatrix}\rho(\tilde{w}-z_t)\\ \rho\tilde{u}(\tilde{w}-z_t)\\ \rho\tilde{v}(\tilde{w}-z_t)\\ \rho\tilde{w}(\tilde{w}-z_t)+p\\ \rho E(\tilde{w}-z_t)+p\tilde{w}\end{bmatrix}$$
$$+\frac{\partial}{\partial x}\begin{bmatrix}0\\ \tilde{\sigma}_{xx}\\ \tilde{\sigma}_{xy}\\ \tilde{\sigma}_{xz}\\ \tilde{u}\tilde{\sigma}_{xx}+\tilde{v}\tilde{\sigma}_{xy}+\tilde{w}\tilde{\sigma}_{xz}+q_x\end{bmatrix}+\frac{\partial}{\partial y}\begin{bmatrix}0\\ \tilde{\sigma}_{xy}\\ \tilde{\sigma}_{yy}\\ \tilde{\sigma}_{yz}\\ \tilde{u}\tilde{\sigma}_{xy}+\tilde{v}\tilde{\sigma}_{yy}+\tilde{w}\tilde{\sigma}_{yz}+q_y\end{bmatrix}+\frac{\partial}{\partial z}\begin{bmatrix}0\\ \tilde{\sigma}_{xz}\\ \tilde{\sigma}_{yz}\\ \tilde{\sigma}_{zz}\\ \tilde{u}\tilde{\sigma}_{xz}+\tilde{v}\tilde{\sigma}_{yz}+\tilde{w}\tilde{\sigma}_{zz}+q_z\end{bmatrix}=0 \tag{1}$$

The FVM is implemented by setting the grid velocities to the negative gust velocities

$$x_t=-\hat{u},\quad y_t=-\hat{v},\quad z_t=-\hat{w} \tag{2}$$

and the energy and pressure are given by

$$E=\frac{p}{\rho(\gamma-1)}+\frac{1}{2}(\tilde{u}^2+\tilde{v}^2+\tilde{w}^2) \tag{3}$$

and

$$p=(\gamma-1)(\rho E-\frac{\rho}{2}(\tilde{u}^2+\tilde{v}^2+\tilde{w}^2)) \tag{4}$$

respectively.

The FVM has been shown to yield accurate results for very thin aerofoils by comparing with exact flat-plate analytical solutions from piston theory and linear steady state values.[15] However, FVM is not backed by any compelling reason or clear description of simplifications and assumptions used in its derivation.

II.B. Split Velocity Method

The Split Velocity Method (SVM) takes a similar approach to FVM by prescribing gust velocities and then solving the equations for the remaining flow field. The SVM is derived from the unsteady Navier-Stokes equations on a fixed mesh (Eq. (5)) and by decomposing velocities and energy as shown in Eq. (6). As the SVM is just a rewritten form of the Navier-Stokes equations without any simplifications and assumptions, it can be formulated in a way that makes it possible to show that the FVM neglects the source terms. The evaluation of the additional source terms is an important aspect of the SVM, as these terms account for the effect of the body on the gust, which is not captured by FVM. It has also been shown previously that the energy variable calculated in the FVM and SVM is not the true total energy.[9] However, the computation of pressure and energy in any CFD code implementing these methods does not need to be altered as the underlying relationship between pressure and the modified energy and velocities remains the same. A strong conservative law form of the 3D Navier-Stokes equations is used in order to accurately capture shocks and separations. The unsteady Navier-Stokes equations are given by

$$\begin{aligned}
&\frac{\partial}{\partial t}\begin{bmatrix} \rho \\ \rho u \\ \rho v \\ \rho w \\ \rho E \end{bmatrix} + \frac{\partial}{\partial x}\begin{bmatrix} \rho u \\ \rho u^2 + p \\ \rho uv \\ \rho uw \\ u(\rho E + p) \end{bmatrix} + \frac{\partial}{\partial y}\begin{bmatrix} \rho v \\ \rho vu \\ \rho v^2 + p \\ \rho vw \\ v(\rho E + p) \end{bmatrix} \\
&+\frac{\partial}{\partial z}\begin{bmatrix} \rho w \\ \rho wu \\ \rho wv \\ \rho w^2 + p \\ w(\rho E + p) \end{bmatrix} + \frac{\partial}{\partial x}\begin{bmatrix} 0 \\ \sigma_{xx} \\ \sigma_{xy} \\ \sigma_{xz} \\ u\sigma_{xx} + v\sigma_{xy} + w\sigma_{xz} + q_x \end{bmatrix} \\
&+\frac{\partial}{\partial y}\begin{bmatrix} 0 \\ \sigma_{xy} \\ \sigma_{yy} \\ \sigma_{zy} \\ u\sigma_{xy} + v\sigma_{yy} + w\sigma_{yz} + q_y \end{bmatrix} + \frac{\partial}{\partial z}\begin{bmatrix} 0 \\ \sigma_{xz} \\ \sigma_{yz} \\ \sigma_{zz} \\ u\sigma_{xz} + v\sigma_{yz} + w\sigma_{zz} + q_z \end{bmatrix} = 0
\end{aligned} \tag{5}$$

The velocity and energy are decomposed as

$$u = \tilde{u} + \hat{\hat{v}} \qquad v = \tilde{v} + \hat{\hat{v}} \qquad w = \tilde{w} + \hat{\hat{w}} \qquad E = \tilde{E} + \hat{\tilde{E}} + \hat{\hat{E}} \tag{6}$$

where $\hat{\hat{u}}$, $\hat{\hat{v}}$ and $\hat{\hat{w}}$ are the gust velocity components and $\hat{\hat{E}}$ is computed by substituting the velocity decompositions into Eq. (3), which after some manipulation gives

$$E = \underbrace{\frac{p}{\rho(\gamma-1)} + \frac{1}{2}(\tilde{u}^2 + \tilde{v}^2 + \tilde{w}^2)}_{\tilde{E}} + \underbrace{(\tilde{u}\hat{\hat{u}} + \tilde{v}\hat{\hat{v}} + \tilde{w}\hat{\hat{w}})}_{\hat{\tilde{E}}} + \underbrace{\frac{1}{2}(\hat{\hat{u}}^2 + \hat{\hat{v}}^2 + \hat{\hat{w}}^2)}_{\hat{\hat{E}}} \tag{7}$$

The pressure remains unchanged from the FVM formulation and is therefore given by Eq. (4). The Navier-Stokes equations for the Split Velocity Method are then obtained by substituting the decompositions

in Eq. (6) into the unsteady Navier-stokes equations given by Eq. (5). This gives

$$\frac{\partial}{\partial t}\begin{bmatrix}\rho\\ \rho(\tilde{u}+\hat{u})\\ \rho(\tilde{v}+\hat{v})\\ \rho(\tilde{w}+\hat{w})\\ \rho(\tilde{E}+\hat{\tilde{E}}+\hat{E})\end{bmatrix}+\frac{\partial}{\partial x}\begin{bmatrix}\rho(\tilde{u}+\hat{u})\\ \rho(\tilde{u}+\hat{u})^2+p\\ \rho(\tilde{u}+\hat{u})(\tilde{v}+\hat{v})\\ \rho(\tilde{u}+\hat{u})(\tilde{w}+\hat{w})\\ (\rho(\tilde{E}+\hat{\tilde{E}}+\hat{E}))(\tilde{u}+\hat{u})\end{bmatrix}$$
$$+\frac{\partial}{\partial y}\begin{bmatrix}\rho(\tilde{v}+\hat{v})\\ \rho(\tilde{v}+\hat{v})(\tilde{u}+\hat{u})\\ \rho(\tilde{v}+\hat{v})^2+p\\ \rho(\tilde{v}+\hat{v})(\tilde{w}+\hat{w})\\ (\rho(\tilde{E}+\hat{\tilde{E}}+\hat{E}))(\tilde{v}+\hat{v})\end{bmatrix}+\frac{\partial}{\partial z}\begin{bmatrix}\rho(\tilde{w}+\hat{w})\\ \rho(\tilde{w}+\hat{w})(\tilde{u}+\hat{u})\\ \rho(\tilde{w}+\hat{w})(\tilde{v}+\hat{v})\\ \rho(\tilde{w}+\hat{w})^2+p\\ (\rho(\tilde{E}+\hat{\tilde{E}}+\hat{E}))(\tilde{w}+\hat{w})\end{bmatrix}$$
$$+\frac{\partial}{\partial x}\begin{bmatrix}0\\ \sigma_{xx}\\ \sigma_{xy}\\ \sigma_{xz}\\ (\tilde{u}+\hat{u})\sigma_{xx}+(\tilde{v}+\hat{v})\sigma_{xy}+(\tilde{w}+\hat{w})\sigma_{xz}+q_x\end{bmatrix}+\frac{\partial}{\partial y}\begin{bmatrix}0\\ \sigma_{xy}\\ \sigma_{yy}\\ \sigma_{yz}\\ (\tilde{u}+\hat{u})\sigma_{xy}+(\tilde{v}+\hat{v})\sigma_{yy}+(\tilde{w}+\hat{w})\sigma_{yz}+q_y\end{bmatrix}$$
$$+\frac{\partial}{\partial z}\begin{bmatrix}0\\ \sigma_{xz}\\ \sigma_{yz}\\ \sigma_{zz}\\ (\tilde{u}+\hat{u})\sigma_{xz}+(\tilde{v}+\hat{v})\sigma_{yz}+(\tilde{w}+\hat{w})\sigma_{zz}+q_z\end{bmatrix}=0 \tag{8}$$

where,

$$\sigma_{xx}=\tfrac{2}{3}\tfrac{\mu}{Re}\left(2\tfrac{\partial\tilde{u}}{\partial x}-\tfrac{\partial\tilde{v}}{\partial y}-\tfrac{\partial\tilde{w}}{\partial z}\right)+\tfrac{2}{3}\tfrac{\mu}{Re}\left(2\tfrac{\partial\hat{u}}{\partial x}-\tfrac{\partial\hat{v}}{\partial y}-\tfrac{\partial\hat{w}}{\partial z}\right)\quad\sigma_{yy}=\tfrac{2}{3}\tfrac{\mu}{Re}\left(2\tfrac{\partial\tilde{v}}{\partial y}-\tfrac{\partial\tilde{u}}{\partial x}-\tfrac{\partial\tilde{w}}{\partial z}\right)+\tfrac{2}{3}\tfrac{\mu}{Re}\left(2\tfrac{\partial\hat{v}}{\partial y}-\tfrac{\partial\hat{u}}{\partial x}-\tfrac{\partial\hat{w}}{\partial z}\right)$$

$$\sigma_{zz}=\tfrac{2}{3}\tfrac{\mu}{Re}\left(2\tfrac{\partial\tilde{w}}{\partial z}-\tfrac{\partial\tilde{v}}{\partial y}-\tfrac{\partial\tilde{u}}{\partial x}\right)+\tfrac{2}{3}\tfrac{\mu}{Re}\left(2\tfrac{\partial\hat{w}}{\partial z}-\tfrac{\partial\hat{v}}{\partial y}-\tfrac{\partial\hat{u}}{\partial x}\right)\quad\sigma_{xy}=\tfrac{\mu}{Re}\left(\tfrac{\partial\tilde{u}}{\partial y}+\tfrac{\partial\tilde{v}}{\partial x}\right)+\tfrac{\mu}{Re}\left(\tfrac{\partial\hat{u}}{\partial y}+\tfrac{\partial\hat{v}}{\partial x}\right)$$

$$\sigma_{xz}=\tfrac{\mu}{Re}\left(\tfrac{\partial\tilde{u}}{\partial z}+\tfrac{\partial\tilde{w}}{\partial x}\right)+\tfrac{\mu}{Re}\left(\tfrac{\partial\hat{u}}{\partial z}+\tfrac{\partial\hat{w}}{\partial x}\right)\quad\sigma_{yz}=\tfrac{\mu}{Re}\left(\tfrac{\partial\tilde{v}}{\partial z}+\tfrac{\partial\tilde{w}}{\partial y}\right)+\tfrac{\mu}{Re}\left(\tfrac{\partial\hat{v}}{\partial z}+\tfrac{\partial\hat{w}}{\partial y}\right)$$

$$q_x=-\tfrac{\mu}{Pr}\tfrac{1}{Re}\tfrac{1}{(\gamma-1)M_\infty^2}\tfrac{\partial T}{\partial x}\quad q_y=-\tfrac{\mu}{Pr}\tfrac{1}{Re}\tfrac{1}{(\gamma-1)M_\infty^2}\tfrac{\partial T}{\partial y}$$

$$q_z=-\tfrac{\mu}{Pr}\tfrac{1}{Re}\tfrac{1}{(\gamma-1)M_\infty^2}\tfrac{\partial T}{\partial z}\quad T=\tfrac{\gamma M_\infty^2 p}{\rho}$$

where, Pr,μ and Re are the Prandtl number, dynamic viscosity and Reynolds number respectively. Separating the applied gust from the rest of the solution and after some manipulation of the terms, the Navier-Stokes

equations are given as

$$\frac{\partial}{\partial t}\begin{bmatrix}\rho\\ \rho\tilde{u}\\ \rho\tilde{v}\\ \rho\tilde{w}\\ \rho\tilde{E}\end{bmatrix}+\frac{\partial}{\partial x}\begin{bmatrix}\rho(\tilde{u}+\hat{\tilde{u}})\\ \rho\tilde{u}(\tilde{u}+\hat{\tilde{u}})+p\\ \rho\tilde{v}(\tilde{u}+\hat{\tilde{u}})\\ \rho\tilde{w}(\tilde{u}+\hat{\tilde{u}})\\ \rho\tilde{E}(\tilde{u}+\hat{\tilde{u}})+p\tilde{u}\end{bmatrix}+\frac{\partial}{\partial y}\begin{bmatrix}\rho\tilde{v}\\ \rho\tilde{u}(\tilde{v}+\hat{\tilde{v}})\\ \rho\tilde{v}(\tilde{v}+\hat{\tilde{v}})+p\\ \rho\tilde{w}(\tilde{v}+\hat{\tilde{v}})\\ \rho\tilde{E}(\tilde{v}+\hat{\tilde{v}})+p\tilde{v}\end{bmatrix}+\frac{\partial}{\partial z}\begin{bmatrix}\rho\tilde{w}\\ \rho\tilde{u}(\tilde{w}+\hat{\tilde{w}})\\ \rho\tilde{v}(\tilde{w}+\hat{\tilde{w}})\\ \rho\tilde{w}(\tilde{w}+\hat{\tilde{w}})+p\\ \rho\tilde{E}(\tilde{w}+\hat{\tilde{w}})+p\tilde{w}\end{bmatrix}$$
$$+\frac{\partial}{\partial x}\begin{bmatrix}0\\ \sigma_{xx}\\ \sigma_{xy}\\ \sigma_{xz}\\ \tilde{u}\sigma_{xx}+\tilde{v}\sigma_{xy}+\tilde{w}\sigma_{xz}+q_x\end{bmatrix}+\frac{\partial}{\partial y}\begin{bmatrix}0\\ \sigma_{xy}\\ \sigma_{yy}\\ \sigma_{yz}\\ \tilde{u}\sigma_{xy}+\tilde{v}\sigma_{yy}+\tilde{w}\sigma_{yz}+q_y\end{bmatrix} \tag{9}$$
$$+\frac{\partial}{\partial z}\begin{bmatrix}0\\ \sigma_{xz}\\ \sigma_{yz}\\ \sigma_{zz}\\ \tilde{u}\sigma_{xz}+\tilde{v}\sigma_{yz}+\tilde{w}\sigma_{zz}+q_z\end{bmatrix}+\begin{bmatrix}0\\ s_m(\hat{\tilde{u}})\\ s_m(\hat{\tilde{v}})\\ s_m(\hat{\tilde{w}})\\ s_e(\hat{\tilde{u}},\hat{\tilde{v}},\hat{\tilde{v}})\end{bmatrix}=0.$$

The source terms are given by

$$s_m(\cdot)=\rho\left\{\frac{\partial\cdot}{\partial t}+(\tilde{u}+\hat{\tilde{u}})\frac{\partial\cdot}{\partial x}+(\tilde{v}+\hat{\tilde{v}})\frac{\partial\cdot}{\partial y}+(\tilde{w}+\hat{\tilde{w}})\frac{\partial\cdot}{\partial z}\right\} \tag{10}$$

$$\begin{aligned}s_e(\hat{\tilde{u}},\hat{\tilde{v}},\hat{\tilde{w}}) &= \tilde{u}s_m(\hat{\tilde{u}})+\tilde{v}s_m(\hat{\tilde{v}})+\tilde{w}s_m(\hat{\tilde{w}})+p\left[\frac{\partial\hat{\tilde{u}}}{\partial x}+\frac{\partial\hat{\tilde{v}}}{\partial y}+\frac{\partial\hat{\tilde{w}}}{\partial z}\right]\\ &+ \sigma_{xx}\frac{\partial\hat{\tilde{u}}}{\partial x}+\sigma_{yy}\frac{\partial\hat{\tilde{v}}}{\partial y}+\sigma_{zz}\frac{\partial\hat{\tilde{w}}}{\partial z}+\sigma_{xy}\left[\frac{\partial\hat{\tilde{v}}}{\partial x}+\frac{\partial\hat{\tilde{u}}}{\partial y}\right]+\sigma_{xz}\left[\frac{\partial\hat{\tilde{w}}}{\partial x}+\frac{\partial\hat{\tilde{u}}}{\partial z}\right]+\sigma_{yz}\left[\frac{\partial\hat{\tilde{w}}}{\partial y}+\frac{\partial\hat{\tilde{v}}}{\partial z}\right]\end{aligned} \tag{11}$$

It is noted that the stress tensors, σ, in SVM are calculated based on velocity derivatives for total velocities u, v and w meaning that they include the gust velocities for the calculation of viscous fluxes. This is to eliminate the introduction of dissipative source terms arising from separating velocity derivatives.

II.C. Numerical implementation in the DLR-TAU code

The FVM is already available in the TAU code.[12] SVM was implemented using this existing method as a basis and then calculating the additional source terms at each iteration. Analytical derivatives are computed, which is possible as all derivatives of the gust are derivatives of prescribed components. This minimises dissipation of source terms and provide more accurate results. Also, as the stress tensors require the total velocity, the velocity gradients were modified to include the gust velocities. A cell-vertex scheme was employed for the spatial discretization and the traditional Jameson dissipation[21] was used to stabilise the scheme. The turbulence model used was the original Spalart-Allmaras one-equation model.[22]

III. Results

Results are presented first for a 2D test case; transonic flow around a NACA 0012 aerofoil and then the implementation is applied to a 3D test case involving a generic wide-body aircraft. Comparison between the FVM and SVM is made for a range of gust lengths at different flight conditions. All simulations were performed using a 1-cosine gust, which takes the shape of

$$\hat{\tilde{v}}=\begin{cases}0 & x<x'-H \qquad x>x'\\ \frac{\hat{\tilde{v}}_{max}}{2}\left(1-\cos\left(\frac{\pi(x-x')}{H}\right)\right) & x'\geq x\geq x'-H\end{cases} \tag{12}$$

where x' is the leading-edge position of the gust and is given by

$$x'=u_{ref}t+x_0. \tag{13}$$

Here, u_{ref} is the reference freestream velocity and x_0 is the position of the leading edge of the gust at time zero. For all the cases, the gusts were prescribed to start just outside the computational domain.

III.A. NACA 0012

All the simulations presented in this section are performed using a NACA 0012 aerofoil at an incidence of 0 degrees. The freestream conditions correspond to a Mach number of 0.7 and a Reynolds number of 9.0×10^6. The computations used the 297×49 C-mesh shown in Figure 1. There are 149 points on the aerofoil surface and the mesh is stretched in the direction normal to the wall. The point distribution is preserved in the wake region.

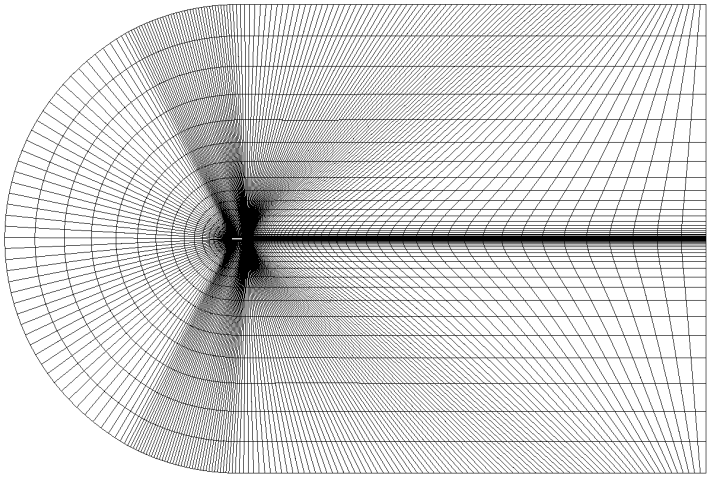

Figure 1. Mesh used for NACA 0012 computations

Both the FVM and SVM were applied to the seven gusts described in table 1.

Table 1. Gust profile data

Case	Gust length (chords)	Gust Velocity (m/s)	Equivalent $\Delta\alpha(deg)$
1	15.47	15.61	3.75
2	61.88	19.69	4.73
3	108.27	21.60	5.18
4	154.67	22.92	5.50
5	5.00	15.61	3.75
6	2.00	15.61	3.75
7	1.00	15.61	3.75

It can be shown that cases 1-4 follow a 1/6th power law meaning longer gusts have larger gust velocities. Cases 5-7 are high-frequency gust cases that are used in this study to determine the effect of gradients on the solutions. The equivalent angle of attack is used to represent the gust velocity as a change in angle of attack and is equal to tan inverse of gust velocity given as a ratio of freestream velocity.

The results are presented using a non-dimensional time given by

$$s = \frac{2u_{ref}t}{c} \tag{14}$$

where t is the physical time step size and c is the chord length, which in this case are $0.005s$ and $1m$, respectively. This represents the number of semi-chords travelled.

The comparison of lift coefficient between FVM and SVM for cases 1-4 are shown in Figure 2 whilst the moment coefficient is shown in Figure 3. These figures show excellent agreement between the two methods for the entire duration of the simulation. This suggests that for these cases the source terms in the SVM are small at all times, which occurs as the gust wavelengths are large enough to ensure that the gradients, which the source terms represent, are small. The shorter wavelength gusts in cases 5-7, have larger gradients and therefore the difference between the FVM and SVM is greater. This is shown by the lift and moment coefficient histories in Figure 4.

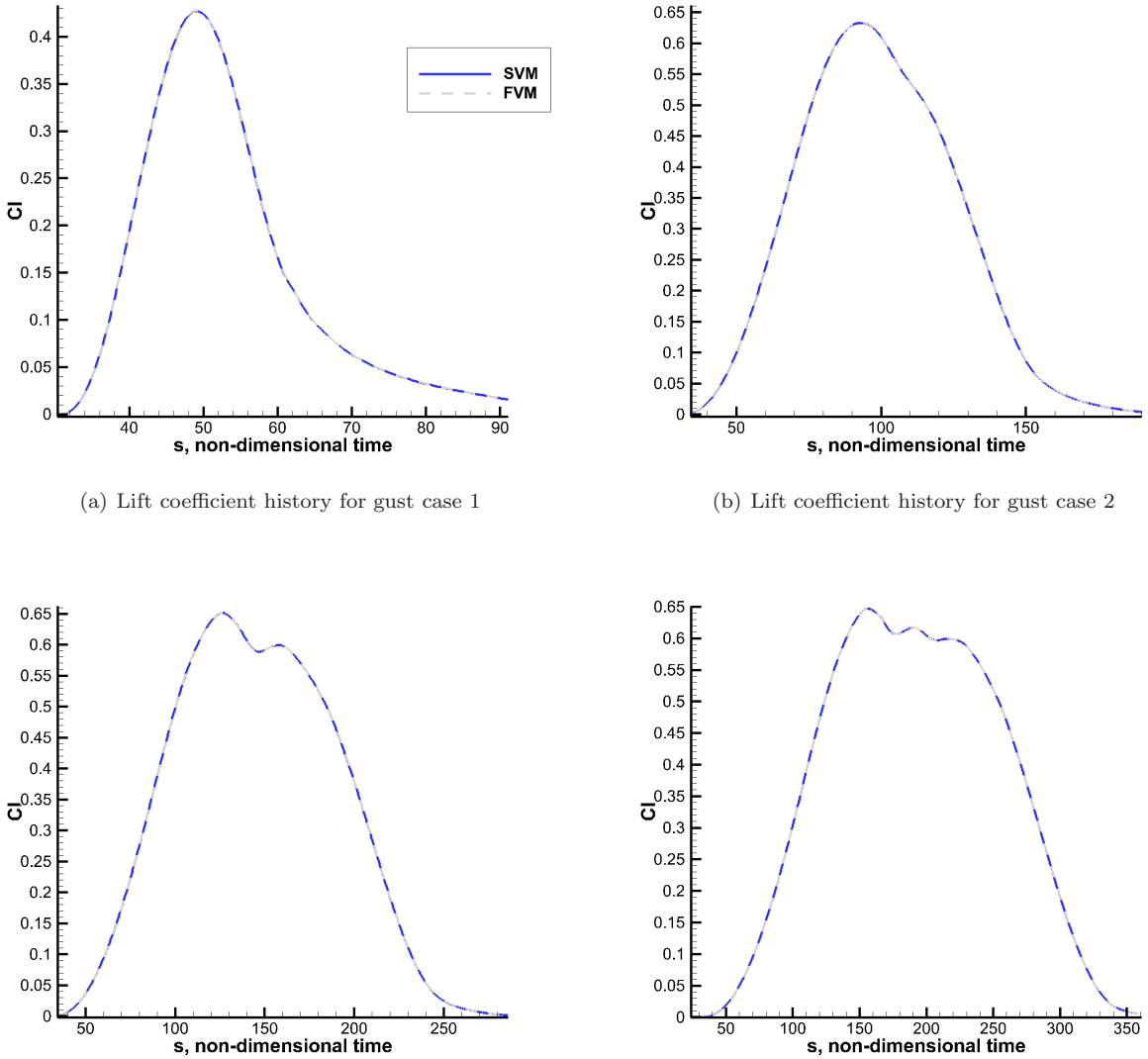

(a) Lift coefficient history for gust case 1

(b) Lift coefficient history for gust case 2

(c) Lift coefficient history for gust case 3

(d) Lift coefficient history for gust case 4

Figure 2. Lift coefficient histories for gust cases 1-4.

From Figure 4 it is clear to see the difference between the two velocity methods. In the shortest wavelength cases the FVM under-predicts the maximum lift and over-predicts the peak lift coefficient values. This is as a result of the method not accounting for the influence of the aerofoil on the gust like the SVM does. It was also found that the difference in the peak lift coefficients calculated by the two methods decreased with increasing gust lengths and that the sum of error values (not absolute value) increased with gust length. The latter is due to the presence of shock-boundary layer interaction that result in movement of shocks and

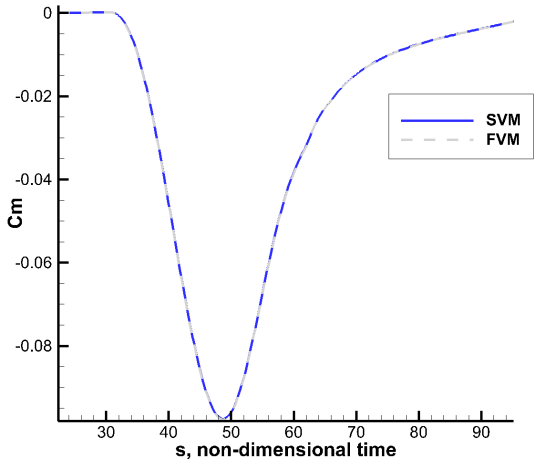

(a) Moment coefficient history for gust case 1

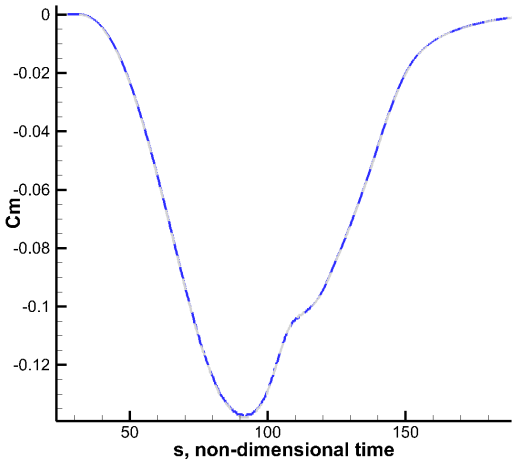

(b) Moment coefficient history for gust case 2

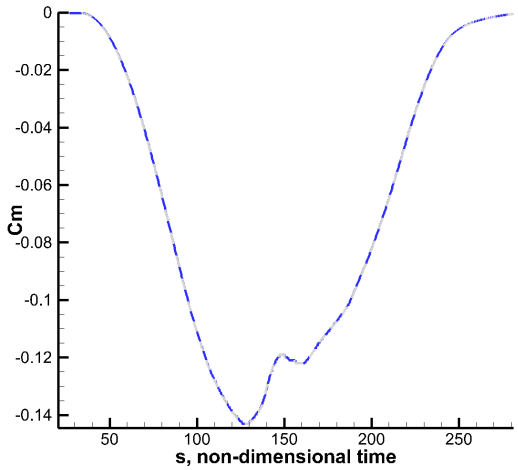

(c) Moment coefficient history for gust case 3

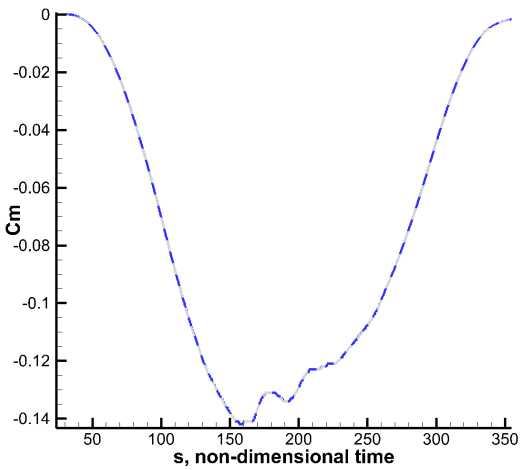

(d) Moment coefficient history for gust case 4

Figure 3. Moment coefficient histories for gust cases 1-4.

separations and therefore affect flow velocity gradients which cause phase lags in lift.

III.B. Wide-body aircraft

Having shown that the SVM provides more accurate results for the simple 2D case for short wavelength gusts, it was then extended to three dimensions. This test involved a half model of a generic wide-body aircraft. An unstructured mesh, generated in SOLAR[23] was used and consisted of 3 million points. Simulations were carried out for the gust profiles and flight conditions as listed in table 2. These gusts were chosen as they represent the shortest, mid-length and longest wavelength gust as specified by the Certification Authorities at different flight conditions. Again the results are presented using the non-dimensional time given in Eq. (14) where a physical time step size of 0.0025s has been used. Lift and moment coefficient results are presented in Figures 5, 6 and 7 for gust simulations at altitudes of 0ft, 29995ft and 43000ft, respectively. These simulations reinforce what was found with the two-dimensional test case. They show that the FVM performs well for longer wavelength gusts but the SVM produces more accurate results at shorter wavelengths. This is due to the inclusion of the effect of the aerofoil on the gust in the SVM that is neglected in the FVM.

Table 2. Gust profile data

Altitude (ft)	Mach Number	Reynolds number	Gust length (m)	Gust Velocity (m/s)	Equivalent $\Delta\alpha(deg)$
0	0.499	11×10^6	18.29	8.825	2.98
0	0.499	11×10^6	91.44	11.540	3.89
0	0.499	11×10^6	213.36	13.290	4.48
29995	0.860	8×10^6	18.29	11.247	2.47
29995	0.860	8×10^6	91.44	14.707	3.23
29995	0.860	8×10^6	213.36	16.938	3.72
43000	0.860	5×10^6	18.29	12.692	2.96
43000	0.860	5×10^6	91.44	16.597	3.87
43000	0.860	5×10^6	213.36	19.114	4.45

For the shortest wavelength gusts at each altitude the second peak corresponds to point where the gust is travelling over the tailplane. This is not evident in the longer wavelength gusts as the wavelength is greater than the distance between the wing and the tailplane. Altitudes of 29995ft and 43000ft provide the greatest difference between the lift coefficient computed by FVM and SVM over the tailplane for the shortest wavelength gust, shown in Figures 6(a) and 7(a). The peak value is over-predicted by the FVM as it does not include any information of the effect of the wing on the gust shape.

IV. Conclusion

The Split Velocity Method for modelling gusts has been derived for viscous flow by rearranging the unsteady Navier-Stokes equations. This showed that the Field Velocity Method is a simplification of the SVM as it neglects the additional source terms found in the SVM. The gust responses for a series of 1-Cosine gusts were compared between the two prescribed velocity methods and the effect of source terms was explored in both two and three dimensions. It was observed that the SVM source terms did not significantly affect solutions for the general gust cases, but did produce noticeable effect on high frequency gusts due to the larger gradients involved. The SVM has been shown to convect gusts and disturbances without dissipation while providing far more insight into flow behaviour and generated forces than the widely used linear panel methods. The SVM allows gusts to be resolved and the mutual interaction if the aircraft and the gust to be simulated without the fine mesh requirement necessary with the FBC method. This allows for detailed modelling at low computational cost thus making it extremely valuable in aircraft design.

Acknowledgments

The research leading to these results was co-funded by Innovate UK, the UKs innovation agency, within the Enhanced Fidelity Transonic Wing project.

References

[1]Khodaparast, H. and Georgiou, G., "Efficient worst case "1-cosine" gust loads prediction," *Journal of Aeroelasticity and Structural Dynamics*, Vol. 2, No. 3, 2012, pp. 33–54.

[2]Hunsaker, J. and Wilson, E., "Report on behavior of aeroplanes in gusts," Tech. Rep. 1, NACA, 1917.

[3]Kussner, H., "Stresses produced in airplane wings by gusts," Tech. rep., NACA, 1932.

[4]Kier, T., "Comparison of unsteady aerodynamic modelling methodologies with respect to flight loads analysis," *AIAA Atmospheric Flight Mechanics Conference and Exhibit*, 2005.

[5]Murua, J., Palacios, R., Michael, J., and Graham, R., "Applications of the unsteady vortex-lattice method in aircraft aeroelasticity and flight dynamics," *Progress in Aerospace Sciences*, Vol. 55, 2012, pp. 46–72.

[6]Cooper, J. and Wright, P., *Introduction to aircraft aeroelasticity and loads*, Wiley-Blackwell, 2008.

[7]Raveh, D., "Gust-response analysis of free elastic aircraft in the transonic flight regime," *Journal of Aircraft*, Vol. 48, No. 4, 2011, pp. 1204–1211.

[8]Barba, L., Leonard, A., and Allen, C., "Vortex method with meshless spatial adaption for accurate simulation of viscous,

unsteady vortical flows," *International Journal for Numerical Methods in Fluids*, Vol. 47, 2005, pp. 841–848.

[9]Wales, C., Gaitonde, A., and Jones, D., "Simulation of airfoil gust rresponse using prescribed velocities," *IFASD*, 2011.

[10]Tang, L. and Baeder, J., "Adaptive euler simulation of supercritical interaction of airfoil and vortex," *AIAA Computational Fluid Dynamics Conference*, 2003.

[11]Tang, L. and Baeder, J., "A two-step grid redistribution method," *Computers & Fluids*, Vol. 32, No. 3, 2003, pp. 323–336.

[12]Heinrich, R. and Reimer, L., "Comparison of different approaches for gust modeling in the CFD code TAU," *International Forum on Aeroelasticity & Structural Dynamics*, 2013.

[13]Sitaraman, J. and Baeder, J., "Field velocity approach and geometric conservation law for unsteady flow simulations," *AIAA Journal*, Vol. 44, 2006, pp. 2084–2094.

[14]Spall, R., "Numerical study of a wing-tip vortex using the euler equations," *Journal of Aircraft*, Vol. 38, 2001, pp. 22–27.

[15]Parameswaran, V. and Baeder, J., "Indicial aerodynamics in compressible flow-direct computational fluid dynamic calculations," *Journal of Aircraft*, Vol. 34, No. 1, 1997, pp. 131–133.

[16]Singh, R. and Baeder, J., "GeneGeneral moving gust response using CFD with application to airfoil-vortex interaction," *15th Applied Aerodynamics Conference*, 1997.

[17]Singh, R. and Baeder, J., "Direct calculation of three-dimensional Indicial lift response using computational fluid dynamics," *Journal of Aircraft*, Vol. 34, 1997, pp. 465–471.

[18]Sitaraman, J., *CFD bbase unsteady aerodynamic modeling for rotor aeroelastic analysis*, Ph.D. thesis, University of Maryland, 2003.

[19]Sitaraman, J. and Baeder, J., "On the field velocity approach and geometric conservation law for unsteady flow simulations," *16th AIAA Computational Fluid Dynamics Conference*, 2003.

[20]Leishman, J., "Subsonic unsteady aerodynamics caused by gusts using the indicial method," *Journal of Aircraft*, 1996.

[21]Jameson, A., Schmidt, W., and Turkel, E., "Numerical Solution of the Euler Equations by Finite Volume Methods Using Runge-Kutta Time-Stepping Schemes," *AIAA paper*, Vol. 81-1259, 1981.

[22]Spalart, P. and Allmaras, S., "A one-equation turbulence model for aerodynamic flows," *AIAA paper*, Vol. 92-0439, 1992.

[23]Martineau, D., Stokes, S., Munday, S., Jackson, A., Gribben, B., and Verhoeven, N., "Anisotropic hybrid mesh generation for industrial RANS applications," *44th AIAA Aerospace Sciences Meeting and Exhibit*, 2006.

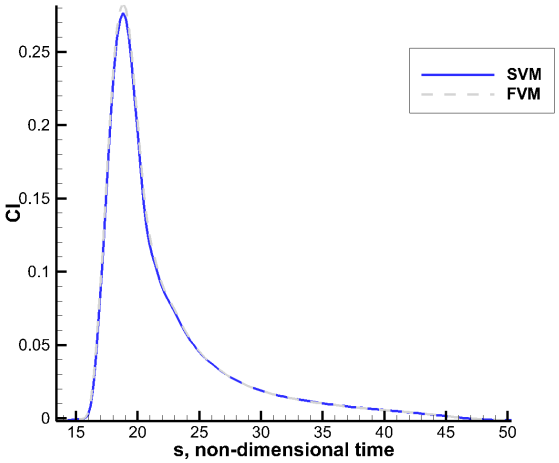

(a) Lift coefficient history for gust case 5

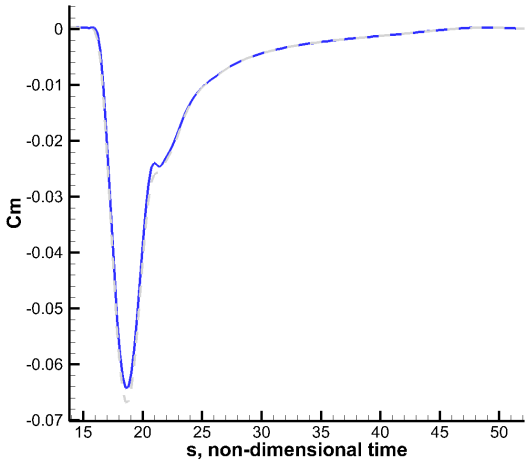

(b) Moment coefficient history for gust case 5

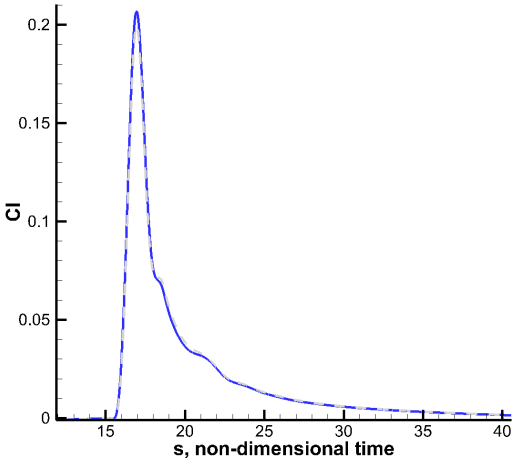

(c) Lift coefficient history for gust case 6

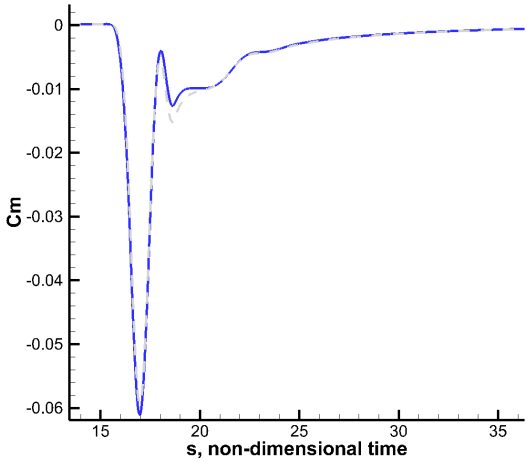

(d) Moment coefficient history for gust case 6

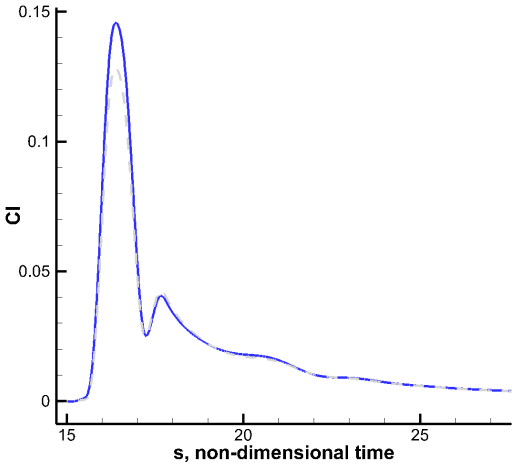

(e) Lift coefficient history for gust case 7

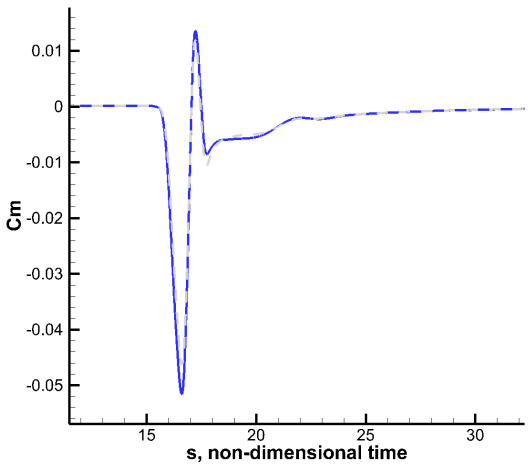

(f) Moment coefficient history for gust case 7

Figure 4. Lift and moment coefficient histories for gust cases 5-7.

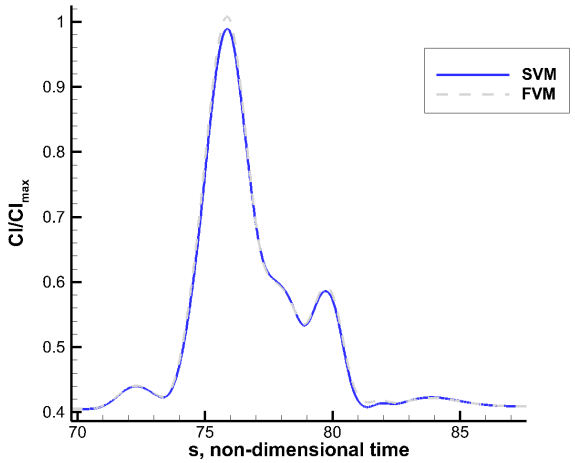

(a) Lift coefficient history an 18.28m wavelength gust

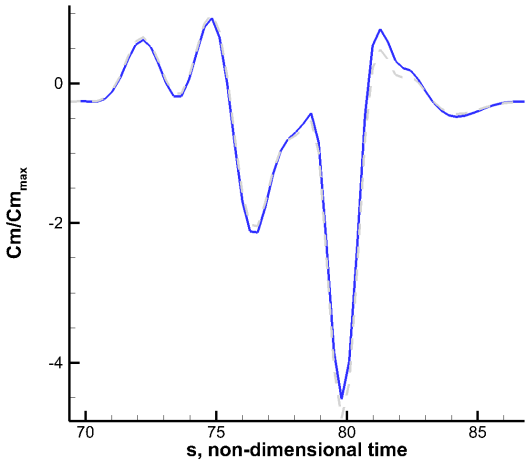

(b) Moment coefficient history an 18.28m wavelength gust

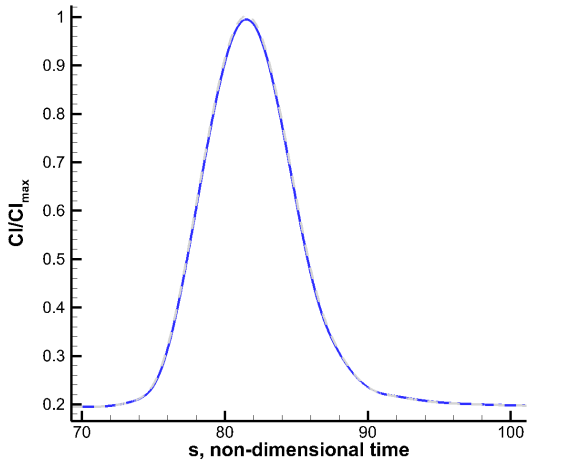

(c) Lift coefficient history an 91.44m wavelength gust

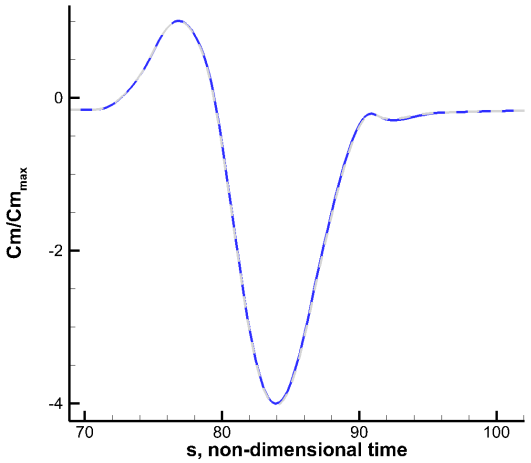

(d) Moment coefficient history an 91.44m wavelength gust

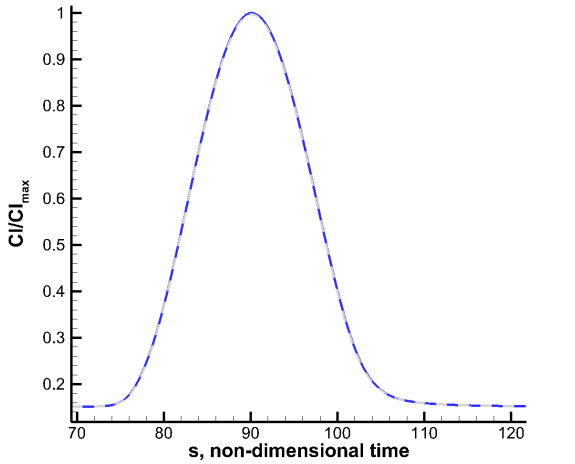

(e) Lift coefficient history an 213.36m wavelength gust

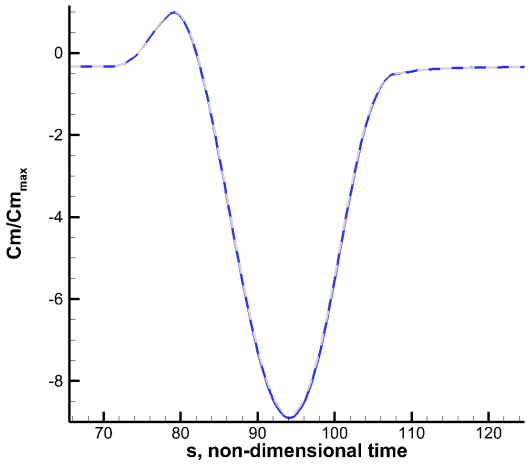

(f) Moment coefficient history an 213.36m wavelength gust

Figure 5. Lift and moment coefficient histories at an altitude of 0ft for different wavelength gusts.

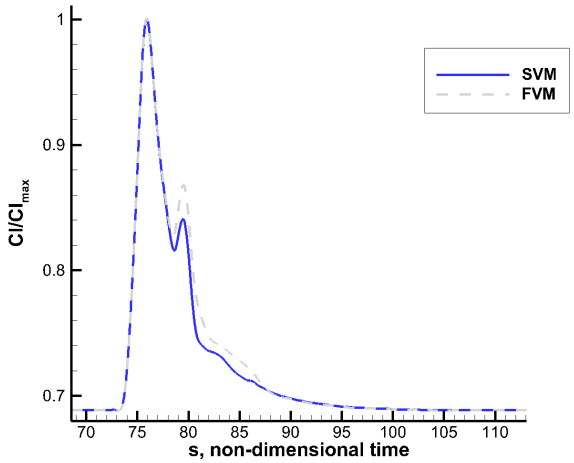

(a) Lift coefficient history an 18.28m wavelength gust

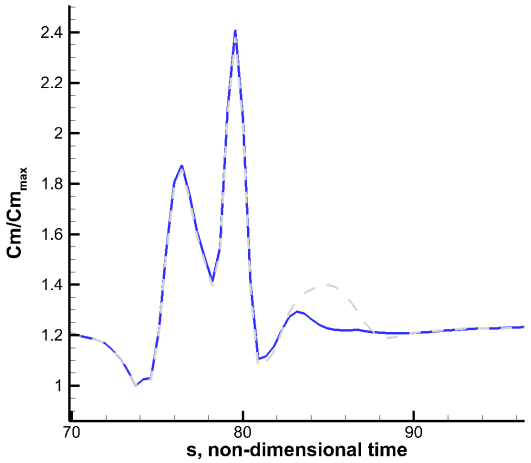

(b) Moment coefficient history an 18.28m wavelength gust

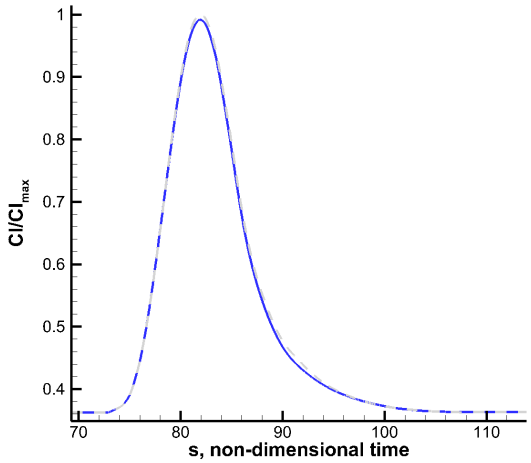

(c) Lift coefficient history an 91.44m wavelength gust

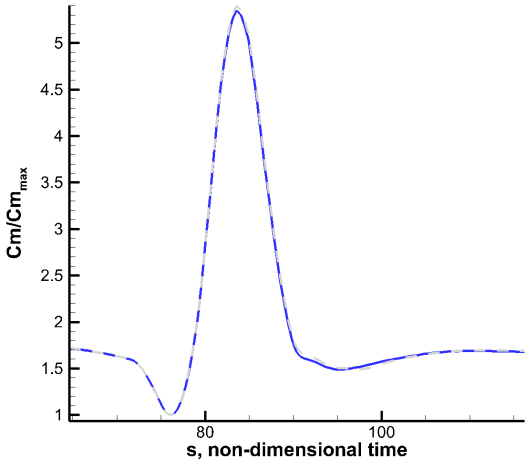

(d) Moment coefficient history an 91.44m wavelength gust

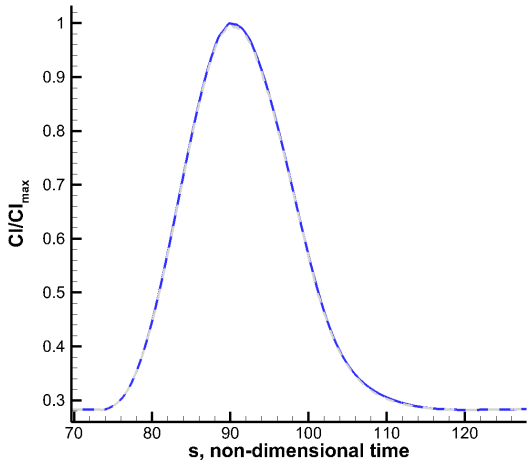

(e) Lift coefficient history an 213.36m wavelength gust

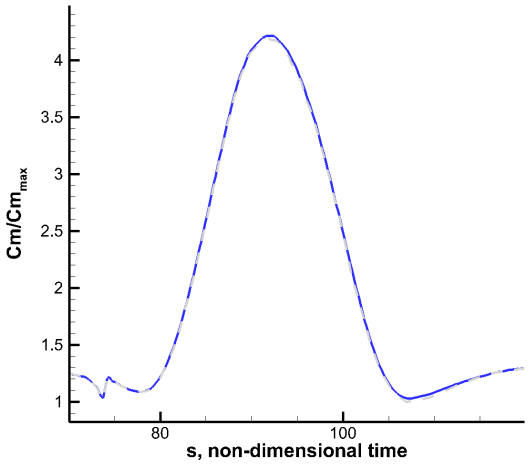

(f) Moment coefficient history an 213.36m wavelength gust

Figure 6. Lift and moment coefficient histories at an altitude of altitude 29995ft for different wavelength gusts.

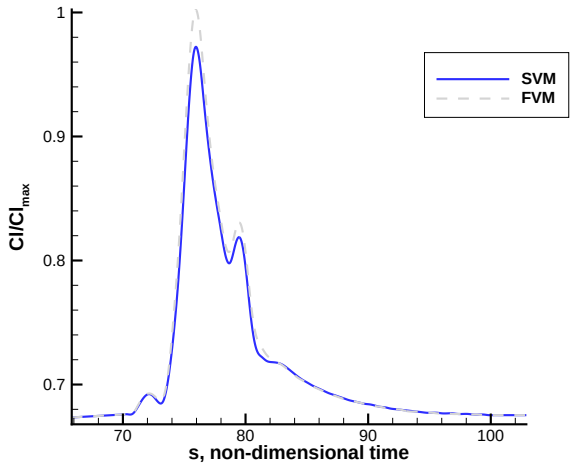

(a) Lift coefficient history an 18.28m wavelength gust

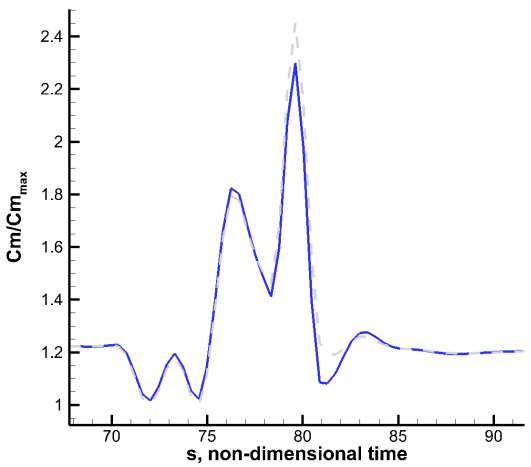

(b) Moment coefficient history an 18.28m wavelength gust

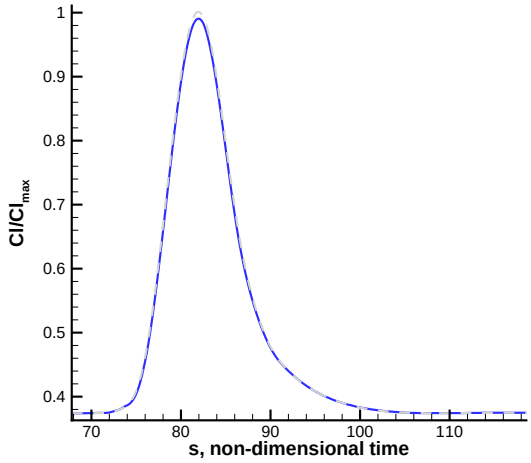

(c) Lift coefficient history an 91.44m wavelength gust

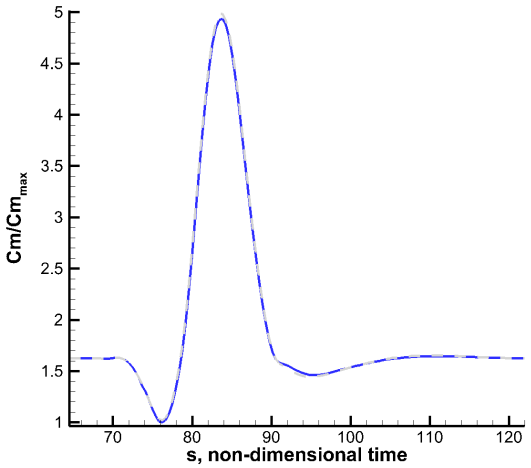

(d) Moment coefficient history an 91.44m wavelength gust

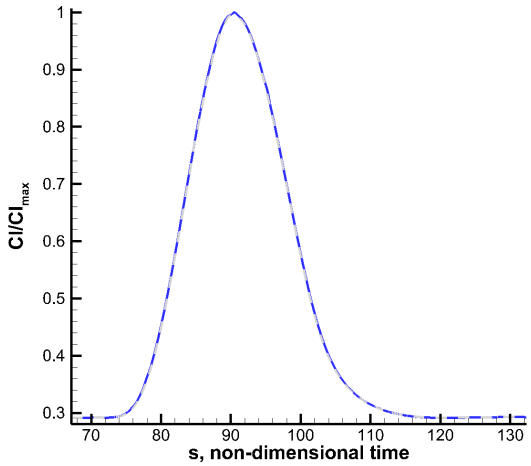

(e) Lift coefficient history an 213.36m wavelength gust

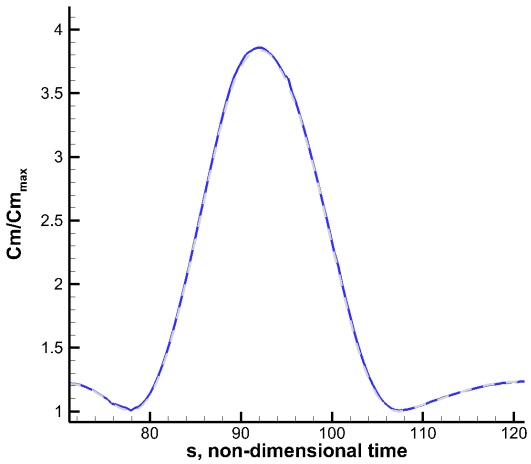

(f) Moment coefficient history an 213.36m wavelength gust

Figure 7. Lift and moment coefficient histories at an altitude of altitude 43000ft for different wavelength gusts.